THE JOURNAL OF PHYSICAL CHEMISTRY A
A JOURNAL OF THE AMERICAN CHEMICAL SOCIETY

pubs.acs.org/JPCA Article

Magneto-Chiral Dichroism and Other Dichroic Spectra of [3]- to [8]Helicenes

Published as part of The Journal of Physical Chemistry A special issue "Forty Years of Response Function Theory".

Janusz Cukras,* Grzegorz Skóra, Jakub Kaminský,* Petr Bouř, Oliwier Misztal, Antoni Tarnowski, and Sonia Coriani

Cite This: *J. Phys. Chem. A* 2025, 129, 11538−11551 Read Online

ACCESS | Metrics & More | Article Recommendations | Supporting Information

ABSTRACT: Magneto-chiral dichroism (MChD) is a fundamental but experimentally elusive chiroptical effect. Carbo[*n*]helicenes, with their strong and systematically evolving chirality, represent ideal systems for its investigation. Here, we present the first theoretical predictions of the MChD spectra for a series of carbo[*n*]helicenes, from [4]- to [8]helicene, calculated using time-dependent density functional theory (TD-DFT) within the damped response framework. To contextualize these predictions and enhance their reliability, we also computed the corresponding electronic circular dichroism (ECD) and magnetic circular dichroism (MCD) spectra, and report the first experimental MCD spectrum of [7]helicene. A systematic scaling procedure, calibrating the computed wavelengths against available experimental ECD and MCD data, was employed to provide reliable estimates for the yet-to-be-measured MChD signals. Our results predict that the MChD signals for larger helicenes, in particular [6]-, [7]-, and [8]helicene, are potentially within the sensitivity of modern experimental setups, with dissymmetry factors (g_{MChD}) of the order of 10^{-6}. An increasing trend in the MChD signal is observed with increasing helicene size, suggesting a correlation with the number of benzene rings. These findings provide a robust theoretical benchmark and are intended to motivate new experimental investigations of this fundamental light−matter interaction.

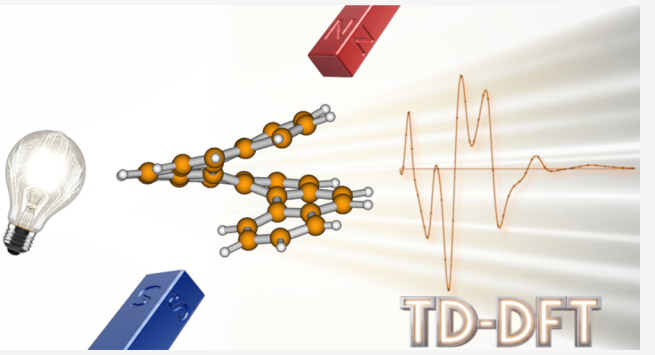

1. INTRODUCTION

Magneto-chiral dichroism (MChD) is a nonreciprocal optical phenomenon observed in chiral media, defined as the difference of absorption of unpolarized light under a static magnetic field, $\vec{B}$, applied parallel versus antiparallel to the propagation vector of light, $\vec{k}$. Its existence, predicted on symmetry grounds and formalized in the early 1980s,[1] was first experimentally confirmed in 1997.[2] The effect is equal in magnitude but opposite in sign for the two enantiomers. MChD is a unique fundamental way in which light and matter interact. It has been elusive experimentally and has sparked interest for a couple of decades.[3−5]

The significance of MChD extends beyond a spectroscopic curiosity. This effect has been proposed for technological applications, such as the optical readout of magnetic data using unpolarized light.[4−6] A reverse effect, where unpolarized light in a magnetic field induces enantiomeric excess in a racemic mixture, has been experimentally demonstrated and is considered a possible mechanism for asymmetric photochemical synthesis on a planetary scale, possibly contributing to the homochirality of life. It is relevant for astrochemical evolution because the two physical entities necessary for its emergence, unpolarized light from stars and magnetic fields from celestial bodies such as planets and neutron stars, are ubiquitous in the universe. The first chiral molecule has been discovered in Crab Nebula.[7,8] However, studying this effect and putting it to use, as mentioned above, is contingent on the discovery and characterization of molecular systems that exhibit a strong MChD response. This challenge underscores the importance of predictive theoretical studies in guiding the measurements of new candidate molecules.

Much of the recent experimental effort to maximize the MChD signal by thoughtful design of molecular systems has focused on paramagnetic, open-shell systems, particularly lanthanide(III) complexes. These ions are targeted for their

Received: September 7, 2025
Revised: November 21, 2025
Accepted: November 24, 2025
Published: December 6, 2025

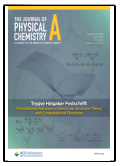

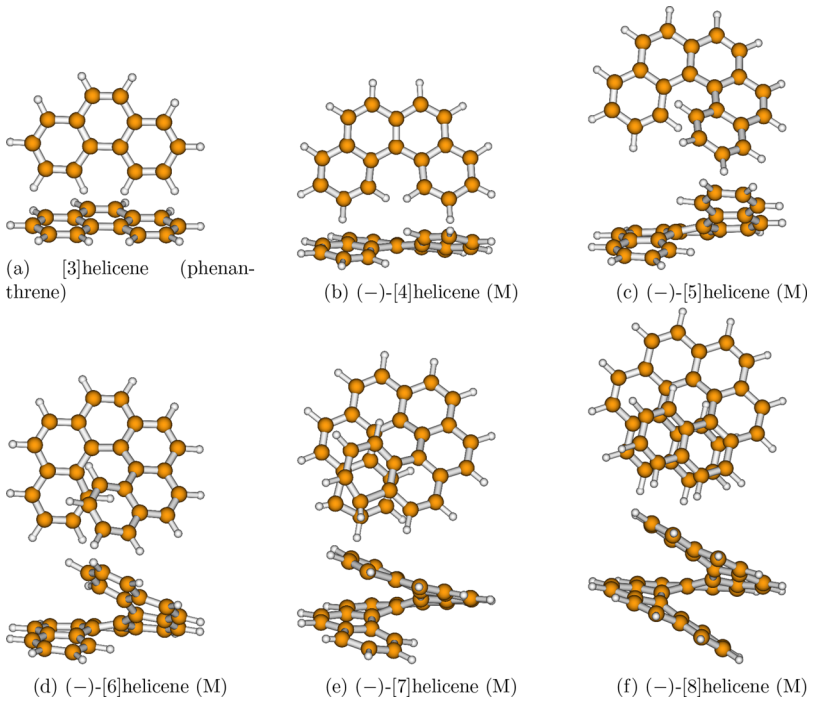

Figure 1. Studied helicenes, viewed from a point along the helix axis and from the side: (a) [3]helicene; (b) [4]helicene; (c) [5]helicene; (d) [6]helicene; (e) [7]helicene; and (f) [8]helicene.

intrinsic properties, such as strong spin−orbit coupling and the presence of magnetic-dipole-allowed f−f transitions, which have recently led to record-high MChD dissymmetry factors.[9−12] However, purely organic, closed-shell molecules remain fundamentally important systems for MChD studies, especially those of biological relevance. Should small chiral organic molecules, such as amino acids, exhibit MChD response, they might provide an argument in the homochirality debate. There is, therefore, a need to extend theoretical predictions to such systems, as we did in our pilot study.[13]

Despite the significance of MChD and progress in the field, experimental MChD investigations are scarce, mainly because the signals are typically very weak or come from exotic systems. This situation creates the need for robust theoretical predictions to identify promising molecular candidates and stimulate experimental efforts. Carbo[*n*]helicenes, a class of ortho-fused polycyclic aromatic hydrocarbons (PAHs), are ideal closed-shell systems for such a study. The steric hindrance causes a strong axial chirality that evolves systematically with the number of fused rings (*n*). Consequently, chiroptical methods, such as electronic circular dichroism (ECD), are routinely used to determine their absolute configuration, while magnetic circular dichroism (MCD) provides a complementary probe of their electronic states. Although the ECD of helicenes has been studied extensively,[14] and their MCD to a lesser extent,[15] their magneto-chiral properties remain unexplored.

Here, we present the first theoretical predictions of MChD spectra for a series of carbo[*n*]helicenes, from [4]- to [8]helicene, calculated using the damped response theory formalism[16−20] as implemented in the DALTON program suite.[13,21,22] To contextualize our primary results and assess the reliability of our computational model, we also calculated the corresponding ECD and magnetic circular dichroism (MCD) spectra. This complementary analysis allows for a comparison with known spectroscopies and enables an empirical adjustment through a rigorous scaling procedure of the calculated MChD results to provide reliable predictions for the yet-to-be-measured MChD signal despite possible model inadequacies. As far as we know, we also report the first experimental MCD spectrum of [7]helicene. Our calculations predict MChD signals for the larger helicenes that are potentially within the reach of modern experimental setups, and we hope that these results will motivate new measurements of this elusive chiroptical effect.

2. COMPUTATIONAL DETAILS

2.1. Structures. The structures of the molecules studied herein are shown in Figure 1. The geometries of (−)-[5]-helicene, (−)-[6]helicene, and (+)-[7]helicene were taken from a study reported in ref 23. They had been optimized *in vacuo* using second-order Møller−Plesset Perturbation Theory with the Dunning-type cc-pVTZ basis set. The structures of [3]helicene (phenanthrene), [4]helicene, and [8]helicene were taken from ref 24. They had been optimized at the B3LYP-D3BJ/def2-TZVP level of theory. No further reoptimization was attempted herein. Based on our analysis and previous work,[14] these different optimization models yield negligible differences in the calculated UV−vis spectra. For consistency, we decided to report all spectra for the M enantiomers. Because the geometry of [7]helicene taken from ref 23 was for the P enantiomer (i.e., (+)-[7]helicene), after performing all the calculations, we vertically flipped (multiplied by −1) the ECD and MChD spectra of this molecule, and used the M geometry in Figure 1e.

2.2. Computational Methodology. For a detailed description of the theory and notation used for the calculation of the response properties and spectra studied in this paper, the reader is referred to ref 13 and the references therein. In general, the properties of interest were obtained from damped response theory[16−20] and transformed into quantities used in

https://doi.org/10.1021/acs.jpca.5c06265
J. Phys. Chem. A 2025, 129, 11538−11551

the experiment, i.e., the molar ellipticities and dissymmetry factors. We applied the computational protocol presented in the aforementioned pilot study (see ref 13), but we will briefly quote in the following the most important aspects and working equations.

The DALTON program suite was used to calculate the properties of interest throughout this study.[21,22] The scripts and data used can be obtained from the authors upon request.

2.2.1. Molar Ellipticities. For circular dichroism effects along an optical path of length l, one observes a difference between the absorptive index, n', for the left-circularly polarized light, n'^{L}, and the absorptive index for the right-circularly polarized light, n'^{R}. Quantitatively, this phenomenon can be encoded in the ellipticity η as follows

$$\eta = \frac{\omega l}{2c_0}\left(n'^{\mathrm{L}} - n'^{\mathrm{R}}\right) \tag{1}$$

where ω is the angular frequency of the incident electromagnetic (EM) wave and c_0 is the speed of the EM wave in vacuum. The molar ellipticity, $[\Theta]$, is obtained by dividing the expression 1 by the concentration of the sample given in 10^{-2} mol/dm^3 and assuming an optical path l = 1 cm. In the following, we present the expressions for the molar ellipticities for each of the studied spectroscopies. A detailed discussion on the units and conversion factors can be found in ref 13.

The molar ellipticity for electronic circular dichroism $[\Theta]^{\mathrm{ECD}}$ was calculated as follows (Einstein's summation convention is assumed throughout):

$$[\Theta]^{\mathrm{ECD}} \approx -\frac{100\omega N_{\mathrm{A}}}{3\epsilon_0 c_0^2} G'_{\alpha\alpha}(g) \tag{2}$$

where N_{A} is Avogadro's constant, ϵ_0 is the electric permittivity of vacuum, and $G'_{\alpha\alpha}(g)$ is the real component of the damped electric dipole−magnetic dipole linear response function:

$$G'_{\alpha\beta}(g) = \mathrm{Re}\langle\langle \mu_\alpha; m_\beta\rangle\rangle^{\gamma}_{\omega} \tag{3}$$

where μ_α is the α component of the electric dipole operator, and m_α is the α component of the magnetic dipole operator, γ is the damping factor and ω is the angular frequency. The notation (g) indicates that the absorptive part of the tensor G' is taken into account.

The magnetic circular dichroism spectra, expressed in terms of the MCD ellipticity $[\Theta]^{\mathrm{MCD}}$, are obtained as follows:

$$[\Theta]^{\mathrm{MCD}} \approx -\frac{25\omega N_{\mathrm{A}}}{3\epsilon_0 c_0} B_z \varepsilon_{\alpha\beta\lambda} \alpha'^{(m)}_{\alpha\beta\lambda}(g) \tag{4}$$

where B_z is magnetic field induction, $\varepsilon_{\alpha\beta\lambda}$ is the Levi-Civita tensor, and $\alpha'^{(m)}_{\alpha\beta\lambda}(g)$ is the real part of the damped quadratic response function:

$$\alpha'^{(m)}_{\alpha\beta\lambda}(g) = -\mathrm{Re}\langle\langle \mu_\alpha; \mu_\beta, m_\lambda\rangle\rangle^{\gamma}_{\omega;0} \tag{5}$$

Although magneto-chiral dichroism spectroscopy is not a circular dichroism spectroscopy, one can *per analogiam* construct a parameter of the MChD ellipticity:

$$[\Theta]^{\mathrm{MChD}} = \frac{\omega l}{2c_0}\left(n'^{\uparrow\uparrow} - n'^{\uparrow\downarrow}\right) \tag{6}$$

where

$$n'^{\uparrow\uparrow} - n'^{\uparrow\downarrow} \approx \frac{N}{3\epsilon_0 c_0} B_z \{B^{A'}(g) + B^{G}(g)\} \tag{7}$$

with

$$B^{A'}(g) = \frac{\omega}{15}\left(3A'^{(m)}_{\alpha,\alpha\beta,\beta}(g) - A'^{(m)}_{\alpha,\beta\beta,\alpha}(g)\right) \tag{8}$$

$$B^{G}(g) = \varepsilon_{\alpha\beta\lambda} G^{(m)}_{\alpha\beta,\lambda}(g) \tag{9}$$

Here, N is the number density of the sample, the tensor $A'^{(m)}$ is the perturbation to the imaginary part of the electric dipole−electric quadrupole optical activity tensor due to an external magnetic field and the tensor $G^{(m)}$ is the perturbation to the real part of the electric dipole−magnetic dipole optical activity tensor. The quadratic response functions needed to calculate them are given as

$$G^{(m)}_{\alpha\beta,\lambda}(-\omega;\omega,0)(g) = \mathrm{Im}\langle\langle \mu_\alpha; m_\beta, m_\lambda\rangle\rangle^{\gamma}_{\omega,0} \tag{10}$$

$$A'^{(m)}_{\alpha,\beta\rho,\lambda}(-\omega;\omega,0)(g) = -\mathrm{Re}\langle\langle \mu_\alpha; \Theta_{\beta\rho}, m_\lambda\rangle\rangle^{\gamma}_{\omega,0} \tag{11}$$

where $\Theta_{\beta\rho}$ denotes the $\beta\rho$ component of the traceless quadrupole moment operator.

For $[\Theta]^{\mathrm{ECD}}$, $[\Theta]^{\mathrm{MCD}}$, and $[\Theta]^{\mathrm{MChD}}$obtained in the manner described above, the conversion from atomic units to deg dm^3 cm^{-1} mol^{-1} was performed using eqs 28, 35, and 39 from ref 13, respectively.

We also modeled the ECD spectrum using conventional (i.e., resonant) response theory yielding excitation energies and rotatory strengths, the so-called stick spectrum. These results are also depicted in the figures with an additional vertical axis for rotatory strength on the right-hand side of the plots. To verify our damped response results, we used Lorentzian broadening for the resultant stick spectrum by employing eqs 15 and 16 from ref 25. An empirical damping factor, corresponding to a Lorentzian broadening of 1000 cm^{-1}, was used to approximate the experimental bandwidths observed in solution and the units are the same as for $[\Theta]^{\mathrm{ECD}}$.

The ECD spectra are often presented as $\Delta\varepsilon$. To compare them with the present results in terms of ellipticities, we used the following relationship (see eq 29 in ref 13 and eq 10 in ref 26):

$$[\Theta](\omega) = \frac{18{,}000\ln(10)}{4\pi}\Delta\varepsilon(\omega) \tag{12}$$

2.2.2. Dissymmetry Factors. We proceed with a brief description of the dissymmetry factors[1,27,28] of the properties studied. For more details and discussion on these values, see ref 13.

The dissymmetry factor for electronic circular dichroism is the difference between n'^{L} and n'^{R} divided by their arithmetic average, yielding:

$$g_{\mathrm{ECD}} = \frac{2(n'^{\mathrm{L}} - n'^{\mathrm{R}})}{(n'^{\mathrm{L}} + n'^{\mathrm{R}})} = -\frac{2G'_{\alpha\alpha}(g)}{c_0 \cdot \alpha_{\alpha\alpha}(g)} \tag{13}$$

The dissymmetry factor for magnetic circular dichroism is the difference in the n' of light of the chosen circular polarization for two opposite directions of magnetic induction B divided by their arithmetic average:

$$g_{\mathrm{MCD}}(B) = \frac{2[n'^{\mathrm{L}}(B) - n'^{\mathrm{L}}(-B)]}{[n'^{\mathrm{L}}(B) + n'^{\mathrm{L}}(-B)]} = -\frac{1}{2}\frac{B_z \varepsilon_{\alpha\beta\lambda}\alpha'^{(m)}_{\alpha\beta\lambda}}{\alpha_{\alpha\alpha}(g)} \tag{14}$$

https://doi.org/10.1021/acs.jpca.5c06265
J. Phys. Chem. A 2025, 129, 11538−11551

In the case of the dissymmetry factor for magneto-chiral dichroism, we take the absorptive indices for the parallel and antiparallel orientations of the magnetic induction and wave vector:

$$g_{\mathrm{MChD}}(B) = \frac{2(n'^{\uparrow\uparrow} - n'^{\uparrow\downarrow})}{(n'^{\uparrow\uparrow} + n'^{\uparrow\downarrow})} = 2\frac{B_z[B^{A'}(g) + B^{G}(g)]}{c_0 \cdot \alpha_{\alpha\alpha}(g)} \tag{15}$$

The denominators of the above relationships contain the polarizability tensor elements $\alpha_{\alpha\alpha}$. They were calculated for the same wavelengths as those used for the properties studied. The dissymmetry factors are dimensionless.

Reports in the literature in refs 14, 15, 29, and 30 did not record the g factors for the studied helicenes but provided dichroic properties of molecules accompanied by their UV−vis spectra. We digitized such data to calculate the g-factor spectrum for a given property using a general relationship:

$$g_{\mathrm{X}} = \frac{\Delta\varepsilon_{\mathrm{X}}}{\varepsilon} \tag{16}$$

where X is ECD, MCD, or MChD.

2.2.3. Basis Sets and Other Details. We considered the correlation-consistent aug-cc-pVDZ basis set of Dunning and co-workers, and its triply augmented variant t-aug-cc-pVDZ.[31,32] However, our study showed that while augmentation itself is important, its level is not. We analyze the dependence on the basis set in an earlier work[13] and herein for the [5]helicene and [6]helicene molecules (see, e.g., Figures S3 and S4). As shown in the figures, the spectra obtained with aug-cc-pVDZ and with t-aug-cc-pVDZ differ only slightly for lower wavelengths. Since these calculations are expensive (10-fold increase in computation time when going from aug- to t-aug-), we limited our study to the smaller basis set. The calculations were performed using the B3LYP functional as the basic choice. For [3]- to [5]helicene, the CAMB3LYP functional was also used for comparison. Since it did not provide qualitatively different results and the scaling procedure described herein sufficed to obtain good agreement between the experiment and computations, we did not use it for larger systems.

The default convergence threshold was used for the energy calculations, whereas a tighter criterion (10^{-6} instead of 10^{-3}) was used for the convergence of the linear response equations. We used an empirical broadening parameter γ of the value 1000 cm^{-1} (0.004556 a.u.). The step between successive frequency points at which the properties were computed was generally set to 0.002 a.u.; for [6]helicene below 0.137 a.u. (338 nm), it was equal to 0.001 a.u. In the case of the ellipticities, these points are presented together with the interpolated spectra. The interpolation was performed using the standard cubic spline method with the help of the Python SciPy module.[33] The dissymmetry factors were obtained from the interpolated data. The strength of the magnetic field was 1 T in all cases.

We did not include solvent effects in this work as this is the first attempt to model MChD spectra for a series of helicenes and our goal was to establish the positions and strengths of the signal within the damped response formalism. Additionally, as stated in other works,[14,15] the vacuum and PCM results for PAHs are very similar.

The calculations of MCD and especially MChD, which require evaluation of quadratic response functions, are very expensive and due to memory limitations require running many separate jobs. To facilitate the management of multiple files and collect results, we developed and tested an in-house Python code that manages these tasks.

Digitization of the spectra from the literature was performed using WebPlotDigitizer[34] and adjustText[35] was used for Figure S8. The pictures of the molecules were prepared using MOLDEN.[36,37]

2.3. Scaling of the Spectra. The calculated transition energies are known to be shifted with respect to the experimental results.[14,15,23] The discrepancy depends on the level of theory. Aside from developing more sophisticated computational protocols, e.g., utilize methods that can describe electron correlation at a higher level, include environmental effects and the influence of molecular vibrations and intermolecular interactions, empirical approaches are often used to improve computational results—that is, the obtained wavelengths are either scaled or shifted. Here, we used both strategies (i.e., scaling and shifting) carefully, based on the available experiments. In other words, the wavelengths calculated from computationally obtained energies were multiplied by a dimensionless scaling factor f_λ and a shifting term Δ_λ in nanometers was added, according to the following expression:

$$\lambda = f_\lambda \cdot \lambda_0 + \Delta_\lambda \tag{17}$$

where λ_0 is the computational wavelength in nm and λ is the final scaled and shifted wavelength in nm.

The procedure to obtain f_λ and Δ_λ is described in detail in the next section. The presentation of the results herein includes both the untreated and scaled spectra. While the fitting procedure was conducted in wavelengths/nanometers, it is important to note that we used the scaled angular frequency values ω obtained from the scaled wavelengths λ to obtain the property values in eqs 2, 4, and 6. This ensures that the values of the properties which depend on the angular frequency of the incident radiation (i.e., the ellipticities) change accordingly. Note that the dissymmetry factors do not depend on the ω values.

There are no experimental MChD results for the studied helicene molecules. Still, we used the scaling factors and shifting terms obtained from ECD and MCD fitting for our MChD calculations since the inadequacies of the chosen theoretical model in reproducing the excitation energy values are the same for ECD, MCD and MChD calculations. While this cannot be said for the property values (intensities), we assume that the amount of scaling needed in all the studied spectroscopies is comparable and hope that such a procedure will provide better prediction of signal positions. This, of course, neglects different experimental conditions of ECD, MCD and hypothetical MChD experiments but one should remember that it has been shown both experimentally and computationally that the influence of the environment on the spectra of helicenes is negligible.[14,15]

2.4. Obtaining the Scaling Factors and Shifting Terms. For a pair of experimental and calculated spectra, the following procedure was performed:

1. A comparison range R for the spectrum was first chosen.
2. Within the comparison range, the data were interpolated, and the spectra normalized according to eq 10 in ref 38. The integral required for normalization was evaluated in SciPy.

https://doi.org/10.1021/acs.jpca.5c06265
J. Phys. Chem. A 2025, 129, 11538−11551

Table 1. Obtained Scaling Factors and Shifting Terms (for Detailed Description, See Text)[a]

helicene	property and method	experiment source	comparison range in nm	max width range in nm	f_λ	Δ_λ in nm	Sim
[4]helicene	MCD, B3LYP/aug-cc-pVDZ	ref 15: Figure 3	221−350	171−450	0.929	17.4	0.437
[4]helicene	MCD, CAMB3LYP/aug-cc-pVDZ	ref 15: Figure 3	221−350	171−425	1.182	−25.7	0.604
[5]helicene	ECD, B3LYP/aug-cc-pVDZ	ref 14: Figure 2	203−350	183−500	0.803	42.9	0.714
[5]helicene	ECD, CAMB3LYP/t-aug-cc-pVDZ	ref 14: Figure 2	203−350	153−500	0.989	15.9	0.703
[5]helicene	ECD, RI-CC2/aug-cc-pVTZ (ref 23: Figure 2)	ref 14: Figure 2	203−350	153−500	0.989	12.6	0.822
[5]helicene	MCD, B3LYP/aug-cc-pVDZ	ref 15: Figure 3	223−375	123−575	0.693	75.8	0.617
[5]helicene	MCD, CAMB3LYP/t-aug-cc-pVDZ	ref 15: Figure 3	223−350	203−500	0.750	83.3	0.609
[6]helicene	ECD, B3LYP/aug-cc-pVDZ	ref 14: Figure 2	201−375	101−525	0.838	29.9	0.845
[6]helicene	ECD, RI-CC2/aug-cc-pVTZ (ref 23: Figure 3)	ref 14: Figure 2	201−375	101−525	0.956	16.7	0.877
[6]helicene	MCD, B3LYP/aug-cc-pVDZ	ref 15: Figure 3	221−365	121−565	0.937	0.5	0.495
[7]helicene	ECD, B3LYP/aug-cc-pVDZ	ref 30: Figure 2	205−405	105−505	0.794	42.0	0.824
[7]helicene	ECD, RI-CC2/aug-cc-pVTZ (ref 23: Figure 4)	ref 30: Figure 2	205−405	105−505	0.887	27.7	0.857
[7]helicene	ECD, B3LYP/aug-cc-pVDZ	ref 42: Figure 1	227−417	127−517	0.738	61.9	0.827
[7]helicene	ECD, RI-CC2/aug-cc-pVTZ (ref 23: Figure 4)	ref 42: Figure 1	227−417	127−517	0.890	29.6	0.862
[7]helicene	MCD, B3LYP/aug-cc-pVDZ	this work	200−400	180−480	0.776	49.5	0.407
[8]helicene	ECD, B3LYP/aug-cc-pVDZ	ref 42: Figure 2	250−440	150−590	0.893	15.9	0.872
[8]helicene	ECD, RI-CC2/TZVPP (ref 14: Figure 2b)	ref 42: Figure 2	265−440	165−540	0.948	20.7	0.975

[a]The constraints in the fitting procedure were defined so as to keep the ends of the calculated spectrum outside the comparison range but within a "max width" range, which was wider than the "comparison range" by a specific margin (its values were 20−200 nm, default 100 nm, chosen to keep the ranges of parameters of maximization (i.e., the scaling factor and shifting term) reasonably narrow and to keep the results of the maximization in agreement with an initial visual analysis of the spectra).

3. The search for the maximum similarity between the two normalized spectra was performed using the basin-hopping algorithm[39] implemented in SciPy.[33] We have tailored the default settings to ensure that the constraints described below are always met.
4. For each of the 10,000 basin-hopping steps, the local maximization of the similarity index was performed (in SciPy[33] as well) using Sequential Least Squares Programming (SLSQP) algorithm.[40] SLSQP was chosen because it enabled the use of constraints to keep the ranges of parameters of maximization (i.e., scaling factors and shifting terms) reasonably narrow and to adjust the ranges to initial visual inspection of the spectra (see Table 1).
5. We selected the similarity index already used for dichroic spectra in the literature (see refs 38 and 41). The general formula is as follows:

$$\mathrm{Sim} = \frac{I_{fg}}{I_{ff} + I_{gg} - |I_{fg}|} \tag{18}$$

where I_{fg} is an overlap integral of the spectra $f(\lambda)$ and $g(\lambda)$ evaluated in the comparison range R:

$$I_{fg} = \int_R f(\lambda) g(\lambda) \mathrm{d}\lambda$$

The evaluation of this integral was performed numerically in SciPy using only the interpolated data.
6. Each fitted spectrum was subsequently subjected to visual evaluation.

3. EXPERIMENTAL SECTION

Commercial heptahelicene (Cymit Química S. L.) was dissolved in *n*-hexane (Sigma-Aldrich) to concentrations of 0.1 mg/mL (~0.26 mM). The absorption, ECD, and MCD spectra were recorded in the 190−400 nm region using a JASCO J-815 spectrometer equipped with a permanent magnet (1.5 T). The spectra were collected at room temperature using a 1 mm Quartz Glass cell (Hellma). The scanning speed was set to 20 nm/min and the response time was 8 s. The final spectra represent the average of three scans. The solvent signal was subtracted, and the spectra were normalized to the path length and concentration, and are presented as molar ellipticities. The MCD spectra were normalized to the magnetic field.

4. RESULTS

A detailed analysis of the types of electronic transitions involved in the studied spectra is discussed in the work of Nakai et al.[14] and of Kaminský et al.[15] In general, helicenes belong to the C_2 symmetry group and the electronic transitions they undergo can be categorized into A and B irreducible representations. The main characteristics of the ECD spectra of these molecules are bisignate positives/negative signals that dominate the spectrum in the lower wavelength region; e.g., for the [6]helicene molecule, these are the prominent signals at 325 and 250 nm. They were characterized as the ^1B_b and ^1B_a bands. Interestingly, the positions of these bands have been linearly correlated with the number $1/n$, where n is the number of benzene rings which can be understood as a metric of the chirality of these systems.[14]

We present both molar ellipticities and dissymmetry factors for the ECD, MCD, and MChD spectra without any fitting (in the Supporting Information) and with the fitting procedure applied as described above. Additionally, we present the scaled optical rotation dispersion (ORD) spectra for [6]-, [7]-, and [8]helicene molecules in Figure S9. In the case of the ellipticities, both the calculated points and the interpolated

https://doi.org/10.1021/acs.jpca.5c06265
J. Phys. Chem. A 2025, 129, 11538−11551

curves are shown. The results and ranges of the search for the scaling factors and shifting terms that maximize the similarity between the calculated and the experimental spectra are listed in Table 1 and presented in Figure S8.

To facilitate a direct comparison with the computed results, the experimental spectra were scaled. For instance, the [Θ] spectrum of Schooley et al.[43] or Vasak et al.,[44] reported without clear units, was multiplied by a factor of the order of 100. The [Θ] spectrum of Martin et al.[42] was scaled by a factor of 10, consistent with Nakai et al.,[14] and some other spectra from literature, e.g., from ref 30, were scaled to match the magnitude of the related experimental data. Notably, the UV−vis spectrum of [7]helicene measured in this work is weaker than those from earlier reports. We observed a similar discrepancy for [5]- and [6]helicenes from ref 15 compared to other experiments. The source of this difference is not immediately apparent. However, scaling both the experimental MCD and the UV−vis spectra ensures that the calculated dissymmetry factors are of the correct order of magnitude for comparison to the experimental values.

4.1. [3]Helicene. Unlike other helicenes, phenanthrene (see Figure 1a), sometimes called [3]helicene, is flat and does not have axial chirality. Hence, we present only the MCD spectra of this molecule. Phenanthrene is included here for completeness and as an additional validation of our approach. To our knowledge, three experimental MCD spectra are available in the literature, by Vašák et al.,[44] by Schooley et al.,[43] and by Kaminský et al.[15] They are reproduced here in Figures 2 and S1. Note that we had to scale the property values from the two former reports because of uncertainty about the units (see figures for details). The experimental spectra show finer details in the region 320−340 nm. This is a vibrational structure studied by Kaminský et al.,[15] which was not considered in our calculations, since the focus here is only on electronic transitions.

The unscaled MCD spectra are presented in Figure S1. The main experimental feature of the spectrum is at approximately 350 nm. The B3LYP predicted wavelength differs from the experiment by approximately 30 nm and CAMB3LYP overestimates the position of this signal even further. One can see that the results obtained with both functionals differ by approximately 15 nm with respect to each other. However, the general features of the spectra are quite similar. This can be seen in Figure 2 where the spectra were scaled according to the procedure described above. The scaled spectra fit well with the experiment except for the strong negative signal predicted at approximately 305 nm. The experiment features only weak negative values in this region. In general, based on the results of Kaminský et al., the calculations appear to overestimate the intensity.

4.2. [4]Helicene. The [4]helicene molecule (see Figure 1b) is the first chiral system in the studied series of molecules. The results for [4]helicene are presented in Figure S2 (unscaled) and 3. Two sets of experimental MCD data[15,43] were included in the plots. Computational ECD results were also reported by Nakai et al.[14] using the second-order approximate coupled-cluster singles and doubles model (CC2) and the resolution-of-identity method. Since we observed a perfect match between the results obtained within the classical response and the damped response theory for the other helicenes, and there is no ECD measurement of [4]helicene available for comparison or fitting, we did not

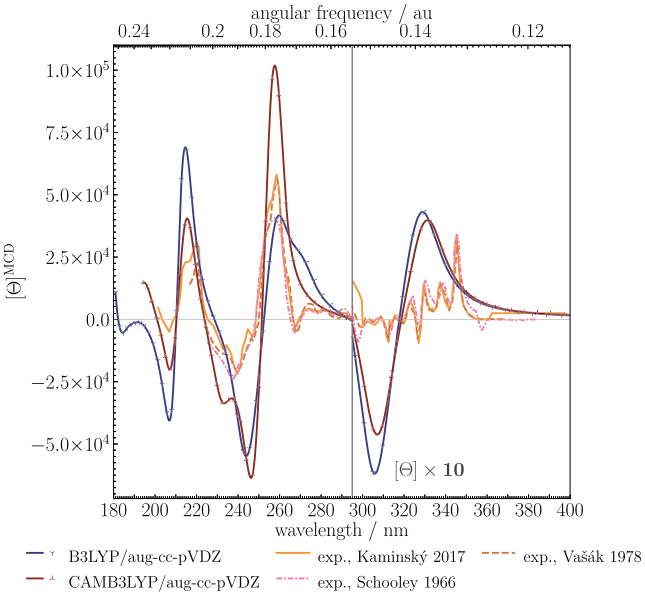

Figure 2. MCD spectrum of phenanthrene ([3]helicene), scaled by visual assessment for the similarity with MCD experimental spectrum by Kaminský et al.;[15] the scaling parameters for B3LYP/aug-cc-pVDZ: f_λ = 1.184, Δ_λ = −43.0 nm and for CAMB3LYP/aug-cc-pVDZ: f_λ = 1.323, Δ_λ = −56.0 nm; the experiments by Schooley et al.[43] and by Vašák et al.[44] were scaled to have values comparable to the experiment of Kaminský et al.; that of Schooley et al. by 2 × 100 (for wavelengths under 269 nm) and 0.5 × 100 (over 269 nm), that of Vašák et al. by 1.5 × 100 (under 269 nm) and 3 × 100 (over 269 nm); all experimental spectra were multiplied by −1. Experimental data reproduced from refs 15 and 44 (Copyright 2017, 1978 American Chemical Society), and ref 43 (Copyright 1966 National Academy of Sciences).

calculate the damped response CAMB3LYP ECD spectrum for [4]helicene.

The unscaled computational ECD spectrum features a weak positive signal at approximately 335 nm and a series of stronger and increasingly negative signals at ca. 285, 255, and 220 nm. The CAMB3LYP results correspond better to the calculations of Nakai et al. than the B3LYP results. In particular, the positive feature at 250 nm is present only in the CAMB3LYP spectrum and the results of Nakai et al.

The scaled computational MCD spectrum fits the experiment well down to 280 nm. However, in the experiment, there are additional features in the region above 280 nm, which appear to be caused by the vibronic structure. We hypothesize that these are the two electronic transitions visible in ECD at ca. 330 and 285 nm, whose vibronic structures overlap in MCD (and are not considered in our calculations). The experimental g_{MCD} spectrum clearly exhibits rich features in this region.

The MChD spectrum presented in Figure 3 was scaled with the factors obtained from the MCD fitting. There are no experimental results available for comparison. We predict g_{MChD} signals of the order of 4×10^{-7} at approximately 275 nm (positive), 265 nm (negative), 225 nm (positive), and 215 nm (negative).

4.3. [5]Helicene. The spectra calculated for [5]helicene are presented in Figure S3 (unscaled), 4, and 5.

In the case of the ECD spectrum, we compare our theoretical results with the experimental spectra registered by Nakai et al.[14] The experimental spectrum in Figure S3 and the

https://doi.org/10.1021/acs.jpca.5c06265
J. Phys. Chem. A 2025, 129, 11538−11551

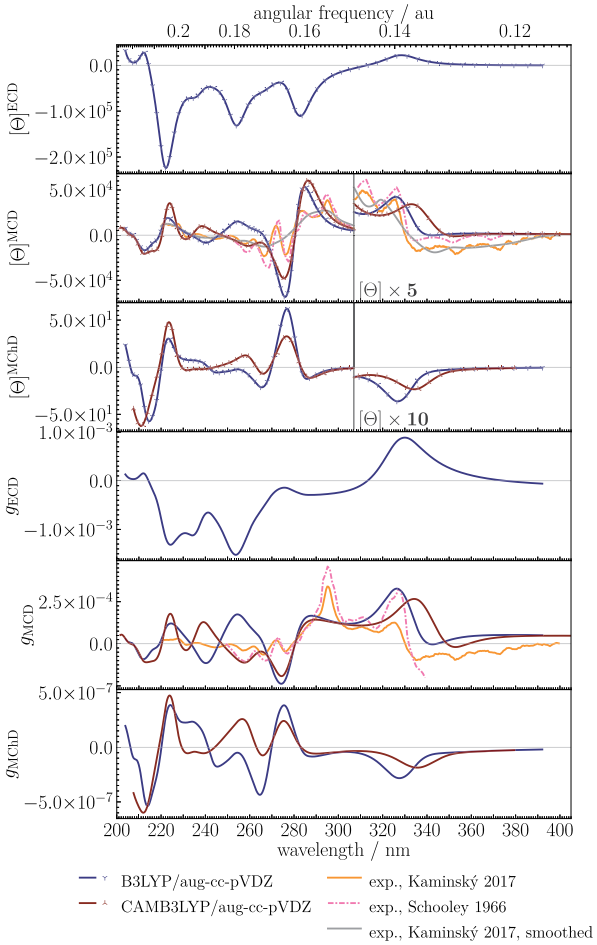

Figure 3. Spectra of [4]helicene, scaled for the highest similarity with MCD experimental spectrum by Kaminský et al.;[15] the scaling parameters for B3LYP/aug-cc-pVDZ spectra are f_λ = 0.929, Δ_λ = 17.3 nm; those for CAMB3LYP/aug-cc-pVDZ are f_λ = 1.182, Δ_λ = −25.6 nm; for illustrative purposes, to suppress the vibronic structure not modeled in this work, the data from Kaminský et al. had been smoothed with the Savitzky−Golay filter (using its implementation in SciPy) and presented as a gray line; both experimental spectra were multiplied by 3; *g* factor for the experiment by Schooley et al.[43] was divided by 3; and the spectrum by Schooley et al. was vertically flipped. Experimental data reproduced from ref 15, (Copyright 2017 American Chemical Society), and ref 43 (Copyright 1966 National Academy of Sciences).

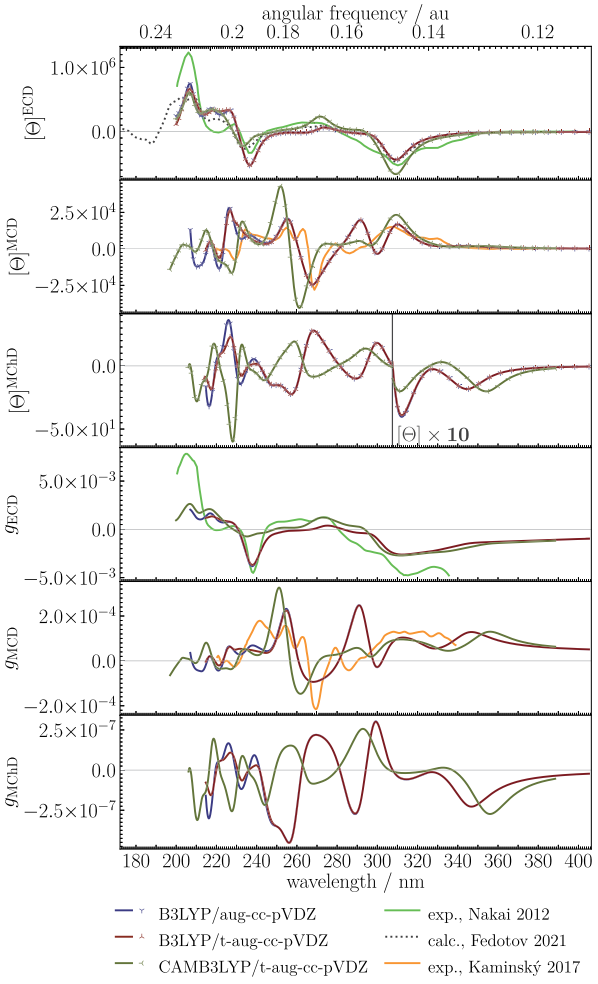

Figure 4. Spectra of [5]helicene, scaled for the highest similarity with ECD experimental spectrum by Nakai et al.;[14] the experimental data were also taken from Kaminský et al.;[15] the scaling parameters for both B3LYP/aug-cc-pVDZ and B3LYP/t-aug-cc-pVDZ spectra are f_λ = 0.803, Δ_λ = 42.9 nm; those for CAMB3LYP/t-aug-cc-pVDZ are f_λ = 0.989, Δ_λ = 15.9 nm; for RI-CC2/aug-cc-pVTZ by Fedotov et al.:[23] f_λ = 0.988, Δ_λ = 12.6 nm; experimental $[\Theta]^{MCD}$ data by Kaminský et al. were multiplied by 2; and data by Nakai et al. were vertically flipped. Experimental data reproduced from refs 15 and 14 (Copyright 2017 and 2012 American Chemical Society). Computational data reprinted from ref 23, with the permission of AIP Publishing.

following figures is multiplied by −1 because we treated the opposite enantiomer in our study. We also transform these data into ellipticities using eq 12. We plot the computational results of Fedotov et al.,[23] which were obtained in the framework of the linear damped response theory using the resolution-of-identity coupled-cluster singles and doubles method (RI-CC2). The RI-CC2 results were also converted to ellipticities using eq 12.

The wavelength of the first prominent experimental feature of the ECD spectrum of [5]helicene, i.e., the structured peak at ca. 310 nm, is overestimated by our unscaled B3LYP results, both in the aug-cc-pVDZ and t-aug-cc-pVDZ basis sets, by approximately 25 nm, and underestimated by CAMB3LYP results by ca. 15 nm. The results of Fedotov et al.[23] show a similar discrepancy.

We conducted the scaling procedure, as described above, to maximize the similarity index between the computational and experimental results. Given that the experimental data for both ECD and MCD are available for [5]helicene, we performed two separate scaling procedures to assess the robustness of our predictions. The first set of spectra was scaled to maximize the similarity with the experimental ECD spectrum from ref 14 and the results are depicted in Figure 4. The second set of spectra was scaled against the experimental MCD spectrum from ref 15. The results of fitting are presented in Figure 5.

The scaled computational ECD spectrum corresponds quite well to the experimental data, although some features at ca. 330 and 340 nm are missing from our results. This discrepancy increases at lower wavelengths.

In the case of the MCD spectrum, we collated our spectra with the measurements by Kaminský et al.[15] The results were reported in $\Delta\varepsilon$ and were converted here into molar ellipticity $[\Theta]^{MCD}$ using eq 12. Kaminský et al. report computational results as well. They employed the sum-over-states (SOS-TDDFT) approach and the complete active space second-

https://doi.org/10.1021/acs.jpca.5c06265
J. Phys. Chem. A 2025, 129, 11538−11551

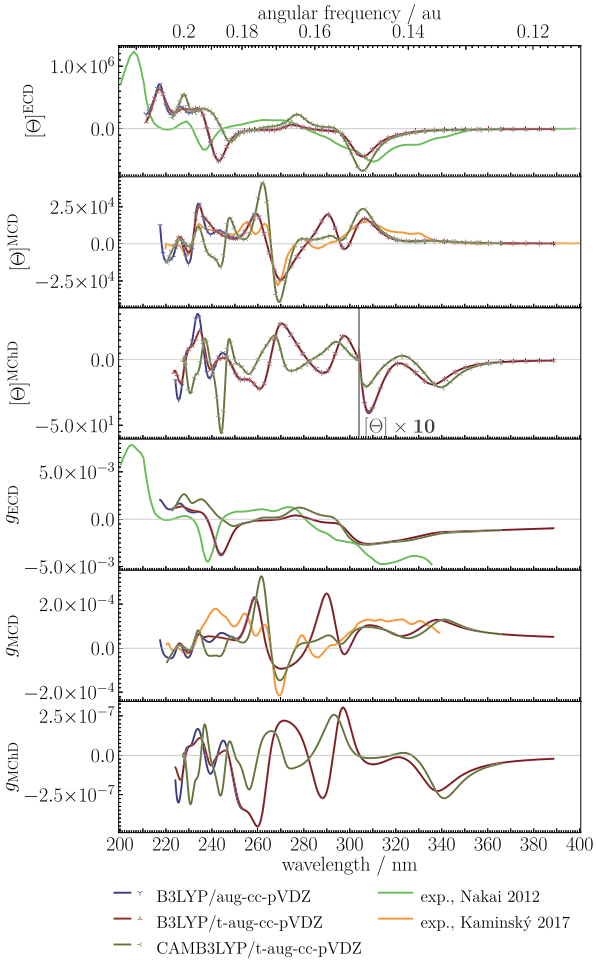

Figure 5. Spectra of [5]helicene, scaled for the highest similarity with MCD experimental spectrum by Kaminský et al.;[15] the experimental data were also take from Nakai et al.;[14] the scaling parameters for both B3LYP/aug-cc-pVDZ and B3LYP/t-aug-cc-pVDZ spectra: f_λ = 0.693, Δ_λ = 75.8 nm, for CAMB3LYP/t-aug-cc-pVDZ: f_λ = 0.750, Δ_λ = 83.3 nm; experimental $[\Theta]^{MCD}$ data by Kaminský et al. were multiplied by 2; and the spectrum by Nakai et al. was vertically flipped. Experimental data reproduced from refs 15 and 14 (Copyright 2017 and 2012 American Chemical Society).

order perturbation theory (CASPT2). However, the authors concluded that the comparison is difficult because of the substantial deviation from the experiment. Hence, we do not include these computational results in our discussion.

The computational spectra scaled so as to maximize the similarity index between the computational and experimental ECD spectra are presented in Figure 4. The scaling factor f_λ for the B3LYP wavelengths was 0.803, and the shifting term was 42.9 nm. For CAMB3LYP, the values were 0.989 and 15.9 nm, respectively (see Table 1). We also scaled the results of Fedotov et al. to quantitatively describe the amount of adjustments required for the different computational results to fit to the experimental data.

An analogous set of spectra obtained by maximizing the similarity index between the computational and experimental MCD spectra is depicted in Figure 5. The scaling factor for B3LYP was 0.693 and the shifting term was 75.8 nm. The fitting for CAMB3LYP yielded 0.750 and 83.3 nm, respectively.

The scaled computational MCD spectrum in terms of molar ellipticities better fits the experimental spectrum than the ECD. The signal at ca. 310 nm is present in the calculation performed with both functionals studied. CAMB3LYP seems to reproduce the features of the spectrum better at higher wavelengths than B3LYP which is exemplified by the spurious strong B3LYP signal at approximately 290 nm. On the other hand, CAMB3LYP overestimates the signal strength at 270 nm.

There are no experimental data for the MChD spectrum of [5]helicene. The MChD computational spectra in Figure 4, scaled using parameters informed by experimental ECD and MCD data, represent, to our knowledge, the first such theoretical predictions for [5]helicene. Note that the $[\Theta]^{MChD}$ spectra above 307 nm are multiplied by a factor of 10, as marked on the plots, with respect to the vertical axis.

On the basis of the obtained scaled g_{MChD} spectra of [5]helicene, utilizing scaling to ECD and MCD experiments, we can offer a prediction that the strongest signal in near-ultraviolet regions are ca. 285−300 nm (positive signal) and ca. 340−365 nm (negative signal). However, the obtained dissymmetry factor is slightly below the previously reported experimental resolution of g (i.e., a few times 10^{-6} T^{-1}[13,45]). Since the first detection, there has been an improvement in the technique to measure the MChD signal,[46] therefore registering these signals is perhaps not beyond the capabilities of modern setups. One of our models, namely the B3LYP functional, predicts that there are even stronger negative signals below 200 nm but this is not confirmed in the CAMB3LYP model.

4.4. [6]Helicene. The results for [6]helicene molecules are presented in Figure S4 (unscaled), 6 and 7. As with the previously discussed helicenes, the experimental results were taken from Nakai et al.,[14] Newman et al.[29] (ECD) and from Kaminský et al.[15] (MCD) and, apart from the not-scaled results (Figure S4), we present two sets of spectra fitted to maximize the similarity index between the theoretical and computational ECD spectra (Figure 6) and the MCD spectra (Figure 7).

In Figure S4, one can see that the first prominent experimental peak of ECD lies at ca. 325 nm. The computational results of Fedotov et al.[23] reproduce this peak very well, while the present calculations performed with the B3LYP functional are off by approximately 25 nm. The calculations by Kaminský et al.[15] using B3LYP/6-311++G** showed a similar shift. Scaling of the computational spectra to fit the experimental ECD (Figure 6) yielded f_λ = 0.838 and Δ_λ = 29.9 nm (see Table 1) and the overall resultant fit of the ECD spectral features is remarkably good.

The first large experimental peak at ca. 325 nm is surrounded by two smaller signals at ca. 350 and 310 nm. Although there are electronic transitions below and above the 350 nm wavelength in our calculations, their rotatory strengths obtained with the employed computational model are too small for the corresponding peaks to become noticeable in the final computational spectrum.

The scaled computational MCD spectrum seems less obvious in comparison to the experiment of Kaminský et al. While the general features seem to be reproduced quite well (the positive and negative trends of the spectrum), there are details in the spectral lines that the computational results lack, e.g., the computational peak between 320 and 350 nm is less clearly resolved into the two signals observed experimentally.

https://doi.org/10.1021/acs.jpca.5c06265
J. Phys. Chem. A 2025, 129, 11538−11551

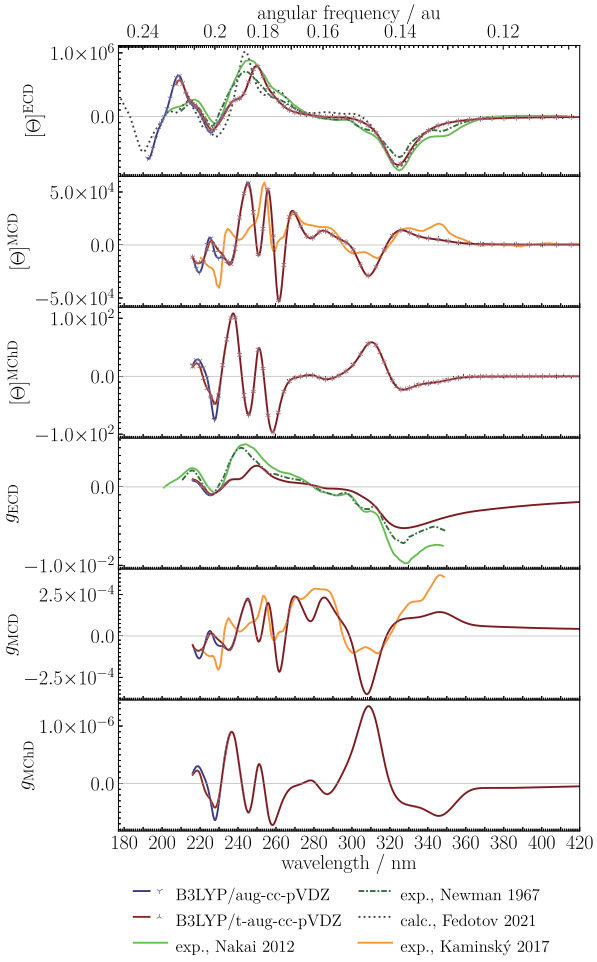

Figure 6. Spectra of [6]helicene, scaled for the highest similarity with ECD experimental spectrum by Nakai et al.;[14] the experimental data were also taken from Newman et al.[29] and Kaminský et al.;[15] the scaling parameters for both B3LYP/aug-cc-pVDZ and B3LYP/t-aug-cc-pVDZ spectra: f_λ = 0.838, Δ_λ = 29.9 nm, for RI-CC2/aug-cc-pVTZ by Fedotov et al.:[23] f_λ = 0.956, Δ_λ = 16.7 nm; experimental $[\Theta]^{MCD}$ data by Kaminský et al. were multiplied by 2; and spectra by Nakai et al. and Newman et al. were vertically flipped. Experimental data reproduced from refs 15, 14, and 29 (Copyright 2017, 2012, and 1967 American Chemical Society). Computational data reprinted from ref 23, with the permission of AIP Publishing.

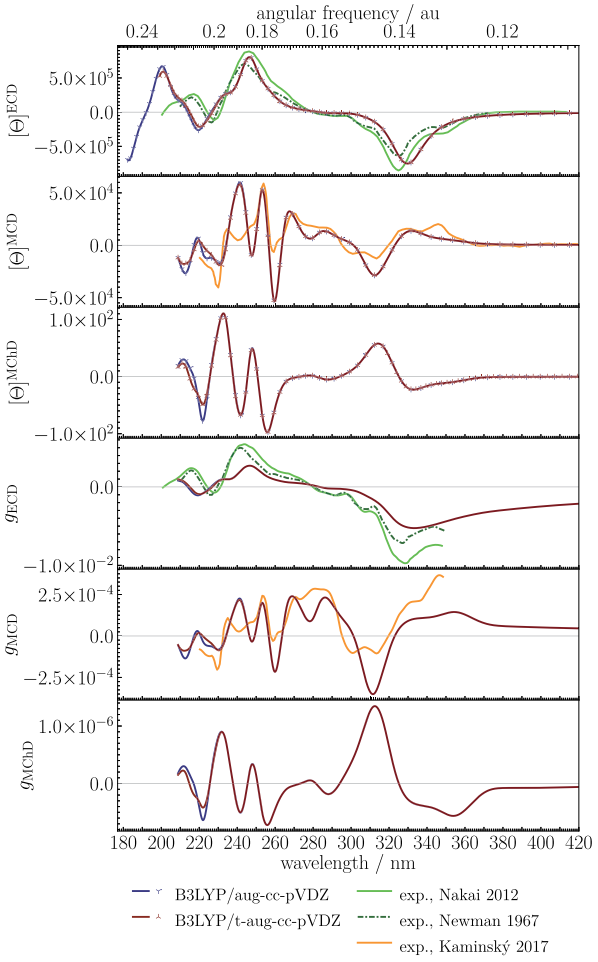

Figure 7. Spectra of [6]helicene, scaled for the highest similarity with MCD experimental spectrum by Kaminský et al.;[15] the experimental data were taken from Nakai et al.,[14] Newman et al.,[29] and Kaminský et al.;[15] the scaling parameters for both B3LYP/aug-cc-pVDZ and B3LYP/t-aug-cc-pVDZ spectra: f_λ = 0.937, Δ_λ = 0.5 nm; experimental $[\Theta]^{MCD}$ data by Kaminský et al. were multiplied by 2; and spectra by Nakai et al. and Newman et al. were vertically flipped. Experimental data reproduced from refs 15, 14, and 29 (Copyright 2017, 2012, and 1967 American Chemical Society).

The negative signal at ca. 310 nm is overestimated, as are the signals in the middle UV range.

Based on the MChD calculations and the scaling performed on the basis of the ECD and MCD experimental results, we predict a fairly strong positive signal in the dissymmetry factor ca. 310−320 nm for the [6]helicene molecule. It is an order of magnitude larger than the largest signal for [5]helicene. One would intuitively expect such a result for a "more chiral" (increased helical turn or helical pitch[14]) molecule.

4.5. [7]Helicene. The ECD, MCD, and MChD spectra of [7]helicene are presented in Figures S5 (unscaled), 8, and 9. There are two ECD experiments available for comparison. One was performed by Brickell et al.[30] and the other by Martin and Marchant.[42] To the best of our knowledge, our measurements of MCD for [7]helicene are the first reported in the literature. For ECD scaling, we chose the wider spectrum of Brickell et al.

In the experimental ECD spectrum there is a broad signal at ca. 350−360 nm, consisting of at least two peaks. Our calculations reproduce only one peak at ca. 410 nm (unscaled) or 360 nm (scaled). The previously reported computational results of Fedotov et al. also reproduced a single peak in this region. The overall trend of the sign of the ECD spectrum is captured well in our calculations, and it changes from positive to negative at ca. 320 nm and then becomes positive again at ca. 250 nm.

At lower energies, the computational MCD spectrum features two bisignate signals, one near 325 nm and another at ca. 300 nm. However, the experiment shows more complicated and broader structures at longer wavelengths. Nevertheless, the entire computational MCD spectrum corresponds well to the experimental spectrum.

Our strongest predicted [7]helicene MChD signal in terms of g_{MChD} lies at a wavelength of approximately 300 nm and exhibits a bisignate line shape. Its positive and negative features are of the same order of magnitude as the strongest signal of [6]helicene, but it is slightly larger: 3×10^{-6} compared to 1.5×10^{-6}.

https://doi.org/10.1021/acs.jpca.5c06265
J. Phys. Chem. A 2025, 129, 11538−11551

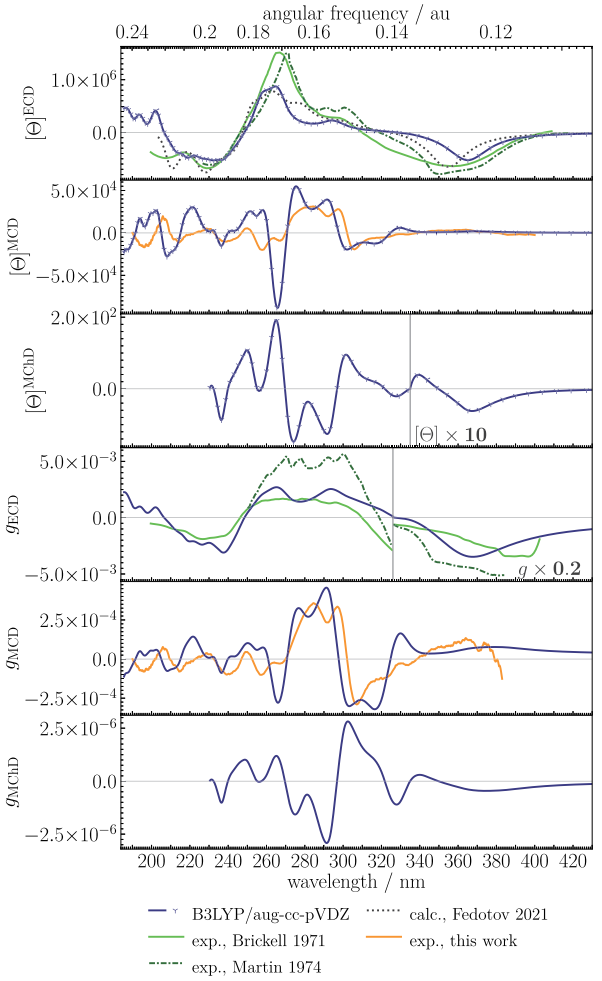

Figure 8. Spectra of [7]helicene, scaled for the highest similarity with ECD experimental spectrum by Brickell et al.;[30] the experimental data were also taken from Martin et al.[42] and from this work; the scaling parameters for B3LYP/aug-cc-pVDZ spectrum: f_λ = 0.794, Δ_λ = 42.0 nm, for RI-CC2/aug-cc-pVTZ data by Fedotov et al.:[23] f_λ = 0.887, Δ_λ = 27.7 nm; experimental $[\Theta]^{ECD}$ data by Brickell et al. were multiplied by 3; experimental $[\Theta]^{ECD}$ data by Martin et al. were multiplied by 10; experimental $[\Theta]^{MCD}$ and experimental g_{MCD} factor obtained in this work were multiplied by 3 and 2, respectively; and spectrum by Fedotov et al. was vertically flipped. Experimental data reprinted with the permission from ref 42 (Copyright 1974 Elsevier), and from ref 30 (Copyright 1971 Royal Society of Chemistry). Computational data reprinted from ref 23, with the permission of AIP Publishing.

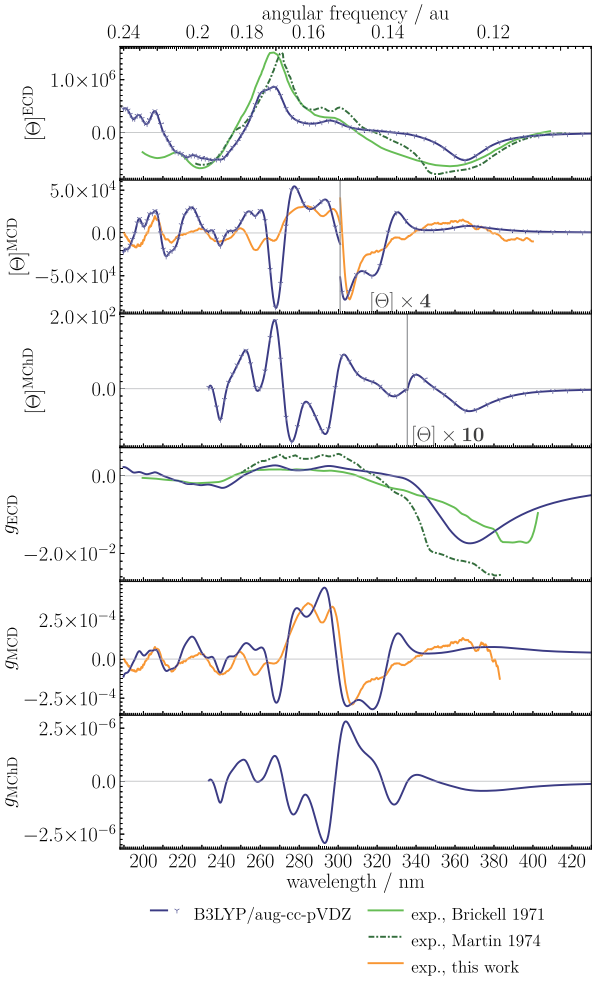

Figure 9. Spectra of [7]helicene, scaled for the highest similarity with MCD experimental spectrum measured in this work; the experimental data were also taken from Brickell et al.[30] and Martin et al.;[42] the scaling parameters for B3LYP/aug-cc-pVDZ spectrum: f_λ = 0.776, Δ_λ = 49.5 nm; experimental $[\Theta]^{ECD}$ data by Brickell et al. were multiplied by 3; experimental $[\Theta]^{ECD}$ data by Martin et al. were multiplied by 10; and experimental $[\Theta]^{MCD}$ and experimental g_{MCD} factor from this work were multiplied by 3 and 2, respectively. Experimental data reprinted with the permission from ref 42 (Copyright 1974 Elsevier), and from ref 30 (Copyright 1971 Royal Society of Chemistry).

4.6. [8]Helicene. The last molecule studied is [8]helicene (see Figure 1f). In this structure, the two planes of the terminal benzene rings face each other. There are two reported ECD experiments[42,47] and one computational study.[14] Together with our results, they are presented in Figures S6 (unscaled) and 10. There are no MCD measurements available in the literature.

The experimental ECD peak at 370 nm is reproduced in the unscaled spectra at 400 nm. Therefore, the functional used underestimates the transition energy by approximately 30 nm. However, the scaled ECD spectrum corresponds well to both experiments.

As for the MCD spectrum, based on the scaled data, we predict that the molecule features a series of signals at about 410, 370, 350, 330, and 310 nm, but stronger signals are present at approximately 285 (positive) and 260 nm (negative).

The scaled MChD computational spectrum in Figure 10 in terms of g_{MChD} exhibits one of the largest MChD signals among the systems studied herein, roughly of the order of 2×10^{-6} which is sufficient for experimental measurements. The strongest signals are observed at 350, 330, 315, 308, and 285 nm.

5. DISCUSSION

We presented ECD, MCD, and especially MChD spectra for a homologous series of helicenes obtained using a damped response TD-DFT approach combined with a systematic scaling procedure, and we presented the first MCD measurements of [7]helicene and the first calculations of the MCD spectrum of [8]helicene.

The choice of the TD-DFT framework for MChD calculations as implemented earlier in DALTON[13] requires the choice of functionals. Although we selected the most

https://doi.org/10.1021/acs.jpca.5c06265
J. Phys. Chem. A 2025, 129, 11538−11551

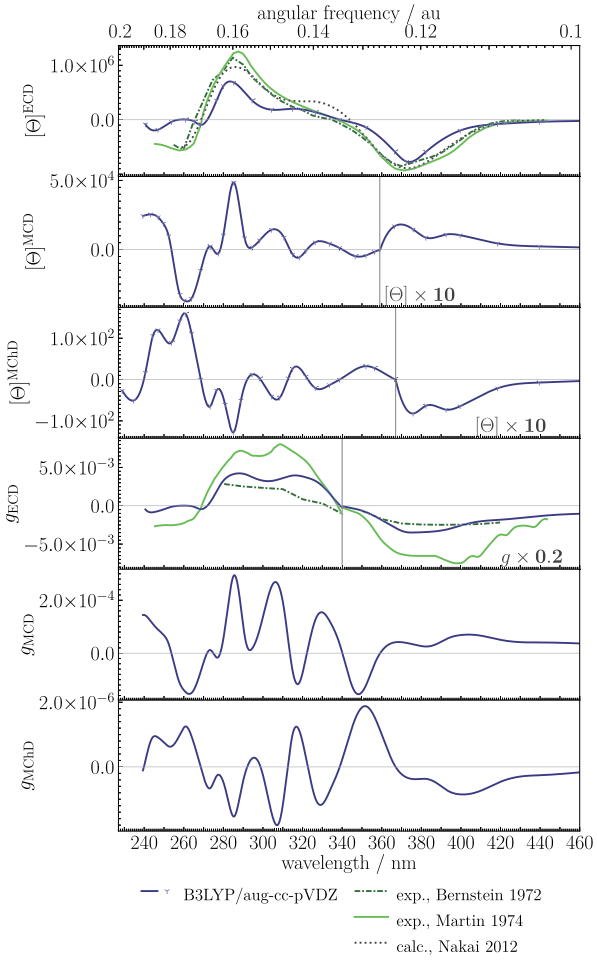

Figure 10. Spectra of [8]helicene, scaled for the highest similarity with ECD experimental spectrum by Martin et al.;[42] the experimental data were also taken from Bernstein et al.;[47] the scaling parameters for B3LYP/aug-cc-pVDZ spectrum: f_λ = 0.893, Δ_λ = 15.9 nm, for RI-CC2/TZVPP by Nakai et al.:[14] f_λ = 0.948, Δ_λ = 20.7 nm; experimental $[\Theta]^{ECD}$ data by Bernstein et al. are multiplied by 3; experimental $[\Theta]^{ECD}$ and g_{ECD} data by Martin et al. were multiplied by 10; and the spectra by Bernstein et al. and by Nakai et al. were vertically flipped. Experimental data reproduced from ref 47 (Copyright 1972 American Chemical Society), and with the permission from ref 42 (Copyright 1974 Elsevier). Computational data reproduced from ref 14 (Copyright 2012 American Chemical Society).

popular functionals, this decision influences the results, as can be seen from the differences between the unscaled B3LYP and CAMB3LYP predictions. The scaling parameters, f_λ and Δ_λ, derived by maximizing the spectral similarity (see Table 1 and Figure S8), reveal consistent trends. Generally, calculations using the B3LYP functional required a larger wavelength scaling (smaller f_λ and larger Δ_λ) compared to the CAMB3LYP or previously reported RI-CC2 results to align with the experimental spectra. This is consistent with the known tendency of B3LYP to underestimate excitation energies. The parameters derived for the RI-CC2 calculations from previous work generally require the least corrections, highlighting their higher accuracy, albeit at a higher computational cost. The scaling parameters of phenanthrene ([3]helicene) and [4]-helicene are somewhat distinct from those of larger helicenes, possibly because of the more significant influence of the vibronic fine structure in the experimental spectra of these smaller, more rigid systems, which was not explicitly modeled here.

The limitations of our model in terms of the choice of the basis set can be observed at shorter wavelengths. The signals in these regions are more susceptible to errors because of the basis set and functional choice.

The calculations were performed *in vacuo*. Although this is a well-established and reasonable approximation for the electronic transitions of PAHs,[14,15] we acknowledge that subtle solvent-specific interactions, unaccounted for here, may contribute to the discrepancies in the scaling factors obtained from the ECD and MCD fitting procedures because the experiments were conducted under different conditions.

The process of scaling and shifting wavelengths, while improving agreement with the experiments, is nonetheless an empirical correction for inherent inaccuracies in predicting excitation energies with the chosen level of theory. We assume that the scaling amends for electronic level errors innate in the method, the solvent effects, subtleties in the spectral structures, intermolecular interactions, etc., all of them at once without any explicit, separate control. This also implies that a perfect match is improbable because all of these inadequacies can be present in all the studied systems to different extents.

Still, the scaled computational ECD and MCD spectra, especially for the larger helicenes, correspond to the experimental spectra very well and generally reproduce the key features adequately. Under the assumption that a similar scaling is needed for the MChD spectra, we can assume that the presented scaled MChD spectra present a prediction of the MChD signal as reliably as for the other presented spectroscopic properties.

A key outcome of this study is the first theoretical prediction of the MChD spectra of [4]- to [8]helicenes. The predicted MChD signal strengths are particularly promising for [6]-, [7]- and [8]helicenes, suggesting that they could be experimentally detected with current or improved setups.

For comparison, in Figure 11, we present our computational results of the dissymmetry factors for the three spectroscopies for all the studied molecules. In this figure, we present the unscaled results since we were unable to scale all the results because of the lack of experiments. From this figure, one can see that there is an overall increasing trend in the signal strength of ECD and MChD with the increasing number of benzene rings, n, in the molecules, while this is not the case for MCD. For ECD, this was reported before.[14,48] Nakai et al.[14] observed that this trend breaks at n = 6. Our observation is similar for n = 7 in the case of ECD. We cannot perform a similar analysis for MChD, indicating specific transitions, because the computational damped response spectrum provides us with the spectral outline and not the strengths for the given transitions. However, visual inspections of the plots in Figure 11 reveals a similar trend in the MChD signals. This trend ends at n = 7, one can see that the signals of [8]helicene are similar to or somewhat smaller than those of [7]helicene. This is probably connected to the fact that, starting from [7]helicene, the benzene rings begin to overlap but the change in this trend needs to be clarified with more research. If the increase in the signal strength of MChD is indeed caused by the increased degree of helical chirality, then perhaps helical structures, for instance α-helical peptides, are in general good candidates for MChD studies. Investigations involving underlying electronic mechanisms, metrics of

https://doi.org/10.1021/acs.jpca.5c06265
J. Phys. Chem. A 2025, 129, 11538−11551

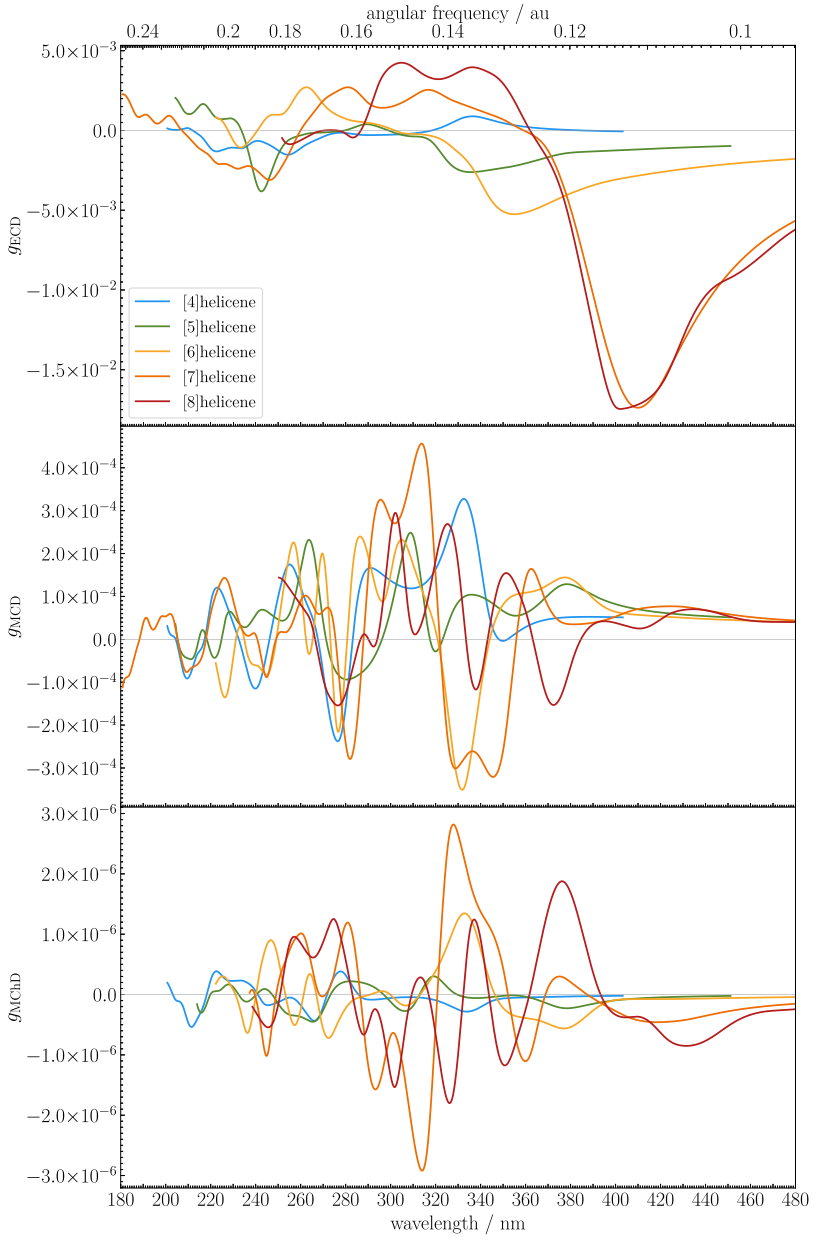

Figure 11. Collected unscaled computational *g*-factor spectra of all the studied helicene molecules.

chirality and helicity seem to be a logical next step we aim to undertake.[49]

As in our previous work,[13] we did not find that the MChD signal can be approximated by $g_{MChD} = g_{ECD} \times g_{MCD}$ (see Figure S10).

Interestingly, for this set of molecules, MCD and MChD are close to mirror reflections of each other. Because MChD flips on the enantiomer change while MCD does not, this means that the MCD and MChD spectra show similar band shapes and relative intensities.

From Figure 11, it can be seen that all the spectra studied are distinct for each helicene molecule. This shows that each of the spectroscopies can be used to distinguish between [*n*]helicenes. The MChD spectra vary significantly from one helicene to another, even though they are the weakest, indicating that they are very sensitive to structural changes. Thus, substituting helicenes may offer pathways for tuning them to enhance the MChD response.

6. CONCLUSIONS

We have modeled the ECD, MCD, and, for the first time, the MChD spectra of carbo[*n*]helicenes from $n = 4$ to $n = 8$ using a damped response TD-DFT methodology. By calibrating our calculations against experimental ECD and MCD data, we provide the first reliable theoretical predictions for the MChD response in this important class of chiral molecules. Our additional calculations of ECD and MCD spectra, performed primarily for context and to establish the reliability of our computational approach, show good qualitative agreement with available experimental data after applying a consistent scaling and shifting procedure to the computed wavelengths.

We have also presented experimental and computational MCD spectrum of [7]helicene for the first time. Moreover, this is the first work to present a computational MCD spectrum of [8]helicene.

https://doi.org/10.1021/acs.jpca.5c06265
J. Phys. Chem. A 2025, 129, 11538−11551

The strongest predicted MChD signals in practical spectral regions in terms of dimensionless dissymmetry factors are as follows:

- [4]helicene: 4×10^{-7} at 275, 265, 225, 215 nm;
- [5]helicene: 3×10^{-7} at 295 and -4×10^{-7} at 260 nm;
- [6]helicene: 1×10^{-6} at 312 nm;
- [7]helicene: 3×10^{-6} at 305 nm and -3×10^{-6} at 295 nm;
- [8]helicene: 2×10^{-6} at 350, 330, 315, 308 nm.

The predicted MChD signals for [6]-, [7]-, and [8]-helicenes are particularly promising, suggesting that they might be experimentally detectable with current or improved setups.

In general, the MChD signal appears to increase with the number of benzene rings in the helicene molecule. This might imply that MChD spectroscopy could be particularly sensitive to the extended helical structures.

The promising results for the larger helicenes presented herein advocate for renewed experimental efforts to measure their magneto-chiral dichroism which would provide a crucial benchmark for theoretical models and advance our understanding for this fundamental chiroptical phenomenon.

■ ASSOCIATED CONTENT

Supporting Information

The Supporting Information is available free of charge at https://pubs.acs.org/doi/10.1021/acs.jpca.5c06265.

Unscaled spectra; measurement of the UV−vis spectrum of the [7]helicene molecule; Optical Rotation Dispersion (ORD) spectra for [6]-, [7]-, and [8]helicene molecules; and $g_{ECD} \times g_{MCD}$ vs g_{MChD} spectra (PDF)

■ AUTHOR INFORMATION

Corresponding Authors

Janusz Cukras − *Faculty of Chemistry, University of Warsaw, 02-093 Warsaw, Poland;* orcid.org/0000-0003-2586-5855; Email: janusz.cukras@uw.edu.pl

Jakub Kaminský − *Institute of Organic Chemistry and Biochemistry, Academy of Sciences, 166 10 Prague, Czech Republic*; Email: jakub.kaminsky@uochb.cas.cz

Authors

Grzegorz Skóra − *Faculty of Chemistry, University of Warsaw, 02-093 Warsaw, Poland;* orcid.org/0000-0001-7685-9143

Petr Bouř − *Institute of Organic Chemistry and Biochemistry, Academy of Sciences, 166 10 Prague, Czech Republic*

Oliwier Misztal − *Faculty of Chemistry, University of Warsaw, 02-093 Warsaw, Poland;* orcid.org/0009-0004-2768-7321

Antoni Tarnowski − *Faculty of Chemistry, University of Warsaw, 02-093 Warsaw, Poland*

Sonia Coriani − *DTU Chemistry, Technical University of Denmark, DK-2800 Kongens Lyngby, Denmark;* orcid.org/0000-0002-4487-897X

Complete contact information is available at: https://pubs.acs.org/10.1021/acs.jpca.5c06265

Notes

The authors declare no competing financial interest.

■ ACKNOWLEDGMENTS

Calculations have been carried out using resources provided by Wroclaw Centre for Networking and Supercomputing (https://wcss.pl), grant No. 321. The authors also thank the Czech Grant Agency (Grant No. 25-15726S). The authors thank the anonymous reviewers for helpful suggestions.

■ REFERENCES

(1) Barron, L.; Vrbancich, J. Magneto-chiral birefringence and dichroism. *Mol. Phys.* **1984**, *51*, 715−730.

(2) Rikken, G. L. J. A.; Raupach, E. Observation of magneto-chiral dichroism. *Nature* **1997**, *390*, 493−494.

(3) Wagnière, G. H. The magnetochiral effect and related optical phenomena. *Chem. Phys.* **1999**, *245*, 165−173.

(4) Atzori, M.; Rikken, G. L. J. A.; Train, C. Magneto-Chiral Dichroism: A Playground for Molecular Chemists. *Chem. Eur. J.* **2020**, *26*, 9784−9791.

(5) Ishii, K.; Hattori, S.; Kitagawa, Y. Recent advances in studies on the magneto-chiral dichroism of organic compounds. *Photochem. Photobiol. Sci.* **2020**, *19*, 9−19.

(6) Atzori, M.; Dhbaibi, K.; Douib, H.; Grasser, M.; Dorcet, V.; Breslavetz, I.; Paillot, K.; Cador, O.; Rikken, G. L. J. A.; Le Guennic, B.; et al. Helicene-Based Ligands Enable Strong Magneto-Chiral Dichroism in a Chiral Ytterbium Complex. *J. Am. Chem. Soc.* **2021**, *143*, 2671−2675.

(7) McGuire, B. A.; Carroll, P. B.; Loomis, R. A.; Finneran, I. A.; Jewell, P. R.; Remijan, A. J.; Blake, G. A. Discovery of the interstellar chiral molecule propylene oxide (CH_3CHCH_2O). *Science* **2016**, *352*, 1449−1452.

(8) Garcia, A. D.; Topin, J.; Bocková, J.; Jones, N. C.; Hoffmann, S. V.; Meinert, C. Chiroptical activity of gas-phase propylene oxide predicting the handedness of interstellar circular polarization in the presolar nebula. *Sci. Adv.* **2022**, *8*, No. eadd4614.

(9) Li, C.-Y.; Adi, L. C.; Paillot, K.; Breslavetz, I.; Long, L.-S.; Zheng, L.-S.; Rikken, G. L. J. A.; Train, C.; Kong, X.-J.; Atzori, M. Enhancement of Magneto-Chiral Dichroism Intensity by Chemical Design: The Key Role of Magnetic-Dipole Allowed Transitions. *J. Am. Chem. Soc.* **2024**, *146*, 16389−16393.

(10) Raju, M. S.; Dhbaibi, K.; Grasser, M.; Dorcet, V.; Breslavetz, I.; Paillot, K.; Vanthuyne, N.; Cador, O.; Rikken, G. L. J. A.; Le Guennic, B.; et al. Magneto-Chiral Dichroism in a One-Dimensional Assembly of Helical Dysprosium(III) Single-Molecule Magnets. *Inorg. Chem.* **2023**, *62*, 17583−17587.

(11) Dhbaibi, K.; Grasser, M.; Douib, H.; Dorcet, V.; Cador, O.; Vanthuyne, N.; Riobé, F.; Maury, O.; Guy, S.; Bensalah-Ledoux, A.; et al. Multifunctional Helicene-Based Ytterbium Coordination Polymer Displaying Circularly Polarized Luminescence, Slow Magnetic Relaxation and Room Temperature Magneto-Chiral Dichroism. *Angew. Chem. Int. Ed.* **2023**, *62*, No. e202215558.

(12) Train, C.; Gheorghe, R.; Krstic, V.; Chamoreau, L.-M.; Ovanesyan, N. S.; Rikken, G. L. J. A.; Gruselle, M.; Verdaguer, M. Strong magneto-chiral dichroism in enantiopure chiral ferromagnets. *Nat. Mater.* **2008**, *7*, 729−734.

(13) Cukras, J.; Johansson, J.; Norman, P.; Rizzo, A.; Rikken, G.; Coriani, S. A Complex-Polarization-Propagator Protocol for Magneto-Chiral Axial Dichroism and Birefringence Dispersion. *Phys. Chem. Chem. Phys.* **2016**, *18*, 13267−13279.

(14) Nakai, Y.; Mori, T.; Inoue, Y. Theoretical and Experimental Studies on Circular Dichroism of Carbo[*n*]Helicenes. *J. Phys. Chem. A* **2012**, *116*, 7372−7385.

(15) Kaminský, J.; Chalupský, J.; Štěpánek, P.; Kříž, J.; Bouř, P. Vibrational Structure in Magnetic Circular Dichroism Spectra of Polycyclic Aromatic Hydrocarbons. *J. Phys. Chem. A* **2017**, *121*, 9064−9073.

(16) Norman, P.; Bishop, D. M.; Jørgen, A.; Jensen, H.; Oddershede, J. Near-resonant absorption in the time-dependent self-consistent field and multiconfigurational self-consistent field approximations. *J. Chem. Phys.* **2001**, *115*, 10323−10334.

(17) Norman, P.; Bishop, D. M.; Jensen, H. J. A.; Oddershede, J. Nonlinear response theory with relaxation: The first-order hyperpolarizability. *J. Chem. Phys.* **2005**, *123*, 194103.
(18) Kristensen, K.; Kauczor, J.; Kjærgaard, T.; Jørgensen, P. Quasienergy formulation of damped response theory. *J. Chem. Phys.* **2009**, *131*, No. 044112.
(19) Norman, P. A perspective on nonresonant and resonant electronic response theory for time-dependent molecular properties. *Phys. Chem. Chem. Phys.* **2011**, *13*, 20519−20535.
(20) Kauczor, J.; Jørgensen, P.; Norman, P. On the Efficiency of Algorithms for Solving Hartree−Fock and Kohn−Sham Response Equations. *J. Chem. Theory Comput.* **2011**, *7*, 1610−1630.
(21) Aidas, K.; Angeli, C.; Bak, K. L.; Bakken, V.; Bast, R.; Boman, L.; Christiansen, O.; Cimiraglia, R.; Coriani, S.; Dahle, P.; et al. The Dalton Quantum Chemistry Program System. *WIREs Comput. Mol. Sci.* **2014**, *4*, 269−284.
(22) Olsen, J. M. H.; Reine, S.; Vahtras, O.; Kjellgren, E.; Reinholdt, P.; Hjorth Dundas, K. O.; Li, X.; Cukras, J.; Ringholm, M.; Hedegård, E. D.; et al. Dalton Project: A Python Platform for Molecular- and Electronic-Structure Simulations of Complex Systems. *J. Chem. Phys.* **2020**, *152*, 214115.
(23) Fedotov, D. A.; Coriani, S.; Hättig, C. Damped (Linear) Response Theory within the Resolution-of-Identity Coupled Cluster Singles and Approximate Doubles (RI-CC2) Method. *J. Chem. Phys.* **2021**, *154*, 124110.
(24) Karton, A. Relative Energies of Increasingly Large [n]Helicenes by Means of High-Level Quantum Chemical Methods. *Mol. Phys.* **2024**, *122*, No. e2241927.
(25) Scott, M.; Rehn, D. R.; Coriani, S.; Norman, P.; Dreuw, A. Electronic Circular Dichroism Spectra Using the Algebraic Diagrammatic Construction Schemes of the Polarization Propagator up to Third Order. *J. Chem. Phys.* **2021**, *154*, No. 064107.
(26) Fahleson, T.; Kauczor, J.; Norman, P.; Santoro, F.; Improta, R.; Coriani, S. TD-DFT Investigation of the Magnetic Circular Dichroism Spectra of Some Purine and Pyrimidine Bases of Nucleic Acids. *J. Phys. Chem. A* **2015**, *119*, 5476−5489.
(27) Rikken, G. L. J. A.; Raupach, E. Enantioselective magnetochiral photochemistry. *Nature* **2000**, *405*, 932−935.
(28) Rikken, G. L. J. A.; Raupach, E. Pure and cascaded magnetochiral anisotropy in optical absorption. *Phys. Rev. E* **1998**, *58*, 5081−5084.
(29) Newman, M. S.; Darlak, R. S.; Tsai, L. L. Optical Properties of Hexahelicene. *J. Am. Chem. Soc.* **1967**, *89*, 6191−6193.
(30) Brickell, W. S.; Brown, A.; Kemp, C. M.; Mason, S. F. π-Electron Absorption and Circular Dichroism Spectra of [6]- and [7]-Helicene. *J. Chem. Soc. A* **1971**, *0*, 756−760.
(31) Dunning, T. H. Gaussian basis sets for use in correlated molecular calculations. I. The atoms boron through neon and hydrogen. *J. Chem. Phys.* **1989**, *90*, 1007−1023.
(32) Kendall, R. A.; Dunning, T. H.; Harrison, R. J. Electron affinities of the first-row atoms revisited. Systematic basis sets and wave functions. *J. Chem. Phys.* **1992**, *96*, 6796−6806.
(33) Virtanen, P.; Gommers, R.; Oliphant, T. E.; Haberland, M.; Reddy, T.; Cournapeau, D.; Burovski, E.; Peterson, P.; Weckesser, W.; Bright, J.; et al. SciPy 1.0: Fundamental Algorithms for Scientific Computing in Python. *Nat. Methods* **2020**, *17*, 261−272.
(34) Rohatgi, A. *WebPlotDigitizer*. https://automeris.io.
(35) Flyamer, I.; Xue, Z.; Colin; Li, A.; Neff, R.; Vazquez, V.; Dicks, S.; Gustafsson, O.; Morshed, N.; Espinoza, J. L. et al. *Phlya/adjustText: 1.3.0*. 2024. https://zenodo.org/records/14019059.
(36) Schaftenaar, G.; Noordik, J. Molden: a pre- and post-processing program for molecular and electronic structures. *J. Comput.-Aided Mol. Des.* **2000**, *14*, 123−134.
(37) Schaftenaar, G.; Vlieg, E.; Vriend, G. Molden 2.0: quantum chemistry meets proteins. *J. Comput.-Aided Mol. Des.* **2017**, *31*, 789−800.
(38) Polavarapu, P. L.; Covington, C. L. Comparison of Experimental and Calculated Chiroptical Spectra for Chiral Molecular Structure Determination. *Chirality* **2014**, *26*, 539−552.
(39) Wales, D. J.; Doye, J. P. K. Global Optimization by Basin-Hopping and the Lowest Energy Structures of Lennard-Jones Clusters Containing up to 110 Atoms. *J. Phys. Chem. A* **1997**, *101*, 5111−5116.
(40) Kraft, D. *A Software Package for Sequential Quadratic Programming*; Tech. Rep. DFVLR-FB 88-28, DLR (formerly DFVLR, Deutsche Forschungs- und Versuchsanstalt für Luft- und Raumfahrt): Germany, 1988.
(41) Shen, J.; Zhu, C.; Reiling, S.; Vaz, R. A Novel Computational Method for Comparing Vibrational Circular Dichroism Spectra. *Spectrochim. Acta A Mol. Biomol. Spectrosc.* **2010**, *76*, 418−422.
(42) Martin, R. H.; Marchant, M. J. Resolution and Optical Properties ([α]max, ord and cd) of Hepta-, Octa- and Nonahelicene. *Tetrahedron* **1974**, *30*, 343−345.
(43) Schooley, D. A.; Bunnenberg, E.; Djerassi, C. Magnetic Circular Dichroism Studies, II. Preliminary Results with Some Aromatic Compounds. *Proc. Natl. Acad. Sci. U.S.A.* **1966**, *56*, 1377−1382.
(44) Vasak, M.; Whipple, M. R.; Michl, J. Magnetic Circular Dichroism of Cyclic π-Electron Systems. 12. Aza Analogs of Phenanthrene. *J. Am. Chem. Soc.* **1978**, *100*, 6867−6871.
(45) Raupach, E.; Rikken, G.; Train, C.; Malézieux, B. Modelling of magneto-chiral enantioselective photochemistry. *Chem. Phys.* **2000**, *261*, 373−380.
(46) Kopnov, G.; Rikken, G. L. J. A. A Multichannel Magneto-Chiral Dichroism Spectrometer. *Rev. Sci. Instrum.* **2014**, *85*, No. 053106.
(47) Bernstein, W. J.; Calvin, M.; Buchardt, O. Absolute Asymmetric Synthesis. I. Mechanism of the Photochemical Synthesis of Non-racemic Helicenes with Circularly Polarized Light. Wavelength Dependence of the Optical Yield of Octahelicene. *J. Am. Chem. Soc.* **1972**, *94*, 494−498.
(48) Uceda, R. G.; Cruz, C. M.; Míguez-Lago, S.; De Cienfuegos, L. A.; Longhi, G.; Pelta, D. A.; Novoa, P.; Mota, A. J.; Cuerva, J. M.; Miguel, D. Can Magnetic Dipole Transition Moment Be Engineered? *Angew. Chem. Int. Ed.* **2024**, *63*, No. e202316696.
(49) Tuvi-Arad, I.; Shalit, Y.; Alon, G. CSM Software: Continuous Symmetry and Chirality Measures for Quantitative Structural Analysis. *J. Chem. Inf. Model.* **2024**, *64*, 5375−5380.

NOTE ADDED AFTER ASAP PUBLICATION

Due to a production error, some math formatting errors were corrected after this paper was published ASAP December 6, 2025. The corrected version was posted December 18, 2025.

https://doi.org/10.1021/acs.jpca.5c06265
J. Phys. Chem. A 2025, 129, 11538−11551